CERN-EP/79-82
24 July 1979

THE PRODUCTION OF HIGH-MOMENTUM Λ^0, $\bar{\Lambda}^0$, $\Lambda^0(1520)$, $\phi(1020)$ AND $\bar{p}$ PARTICLES IN pp COLLISIONS AT $\sqrt{s}$ = 63 GeV

M.M. Block, G.J. Bobbink, M. Botje,
R. Campanini, M.A. van Driel, F.C. Erné,
D. Favart, W.G.J. Langeveld, P. Leleux,
H.W. Ludwig, P. Kooijman, J.C. Sens,
J. Timmer*) and D. van Wezep

Amsterdam-Louvain-Northwestern Collaboration

ABSTRACT

Data are reported on the momentum distribution of Λ^0, $\bar{\Lambda}^0$, $\Lambda^0(1520)$, $\phi(1020)$, and $\bar{p}$ particles inclusively produced at 1° with respect to the primary beams at the CERN Intersecting Storage Rings. The momentum dependence of the production of these fragments of the proton is discussed in terms of counting rules.

Paper submitted to the
EPS International Conference on High-Energy Physics,
Geneva, 27 June-4 July 1979.

*) Scientific Associate, CERN, Geneva, Switzerland.

1. INTRODUCTION

Data have been taken at the CERN Intersecting Storage Rings (ISR), at a c.m. energy $\sqrt{s}$ = 63 GeV, on

$$\begin{aligned} p + p \rightarrow \pi^- &+ p + X \\ \pi^+ &+ \bar{p} + X \\ K^- &+ p + X \\ K^+ &+ K^- + X \ , \end{aligned}$$

where both detected particles enter one forward spectrometer. The effective mass spectra reveal peaks at the Λ^0, $\bar{\Lambda}^0$, $\Lambda^0(1520)$ and $\phi(1020)$ mass. As yet unnormalized invariant cross-sections have been computed for these particles. In addition, the reaction $p + p \rightarrow \bar{p} + X$ has been measured. The x-distributions are discussed.

2. EQUIPMENT

One of two forward spectrometers, located on the downstream ends of an ISR intersection, is used for this investigation. A figure of the apparatus is shown in a companion paper[1].

Each spectrometer consists of: a septum magnet with a 20 × 30 cm^2 aperture and a 2 T•m magnetic field integral at full excitation; 5 modules of drift chambers with 250 sense wires distributed over 24 planes; 5 trigger counters; one 10-element and one 16-element hodoscope. The two-particle trigger requires at least two elements in each hodoscope to fire. The particles are identified in three atmospheric Čerenkov counters Č1, Č2, and Č3. The counters Č2 and Č3 have split mirrors and two phototubes.

The angular range covered by the spectrometer is 17-39 mrad vertically and ±20 mrad horizontally. The acceptance is $\sim$ 1 msr. The momentum resolution dp/p is $\sim$ 1% at p = 30 GeV/c and maximum magnetic field.

3. DATA-TAKING AND ANALYSIS

The two-particle data to be discussed have been taken with 30-60% of the maximum field and two different trigger conditions:

i) Č1 and Č3 filled with CO_2 with π/K/p thresholds at 4.6/16.2/30.9 GeV/c; Č2 filled with 50% N_2/50% Ne with π/K/p thresholds at 7.5/26.5/50.1 GeV/c. Magnetic field at 30 and 60%.

In these runs all mass peaks discussed were present.

ii) Č1 and Č3 filled with FC114 with π/K/p thresholds at 2.6/9.0/17.1 GeV/c; Č2 filled with CO_2. Magnetic field at 50%.

In these runs Č1 and Č3 were in coincidence in the trigger and Č2 in anti-coincidence. In this way the rate of uniquely identified K^+ mesons at momenta between 9 and 17 GeV is enhanced. In these runs clearer signals of the two-particle states to be discussed were seen.

About 10% of the triggers could be reconstructed as coming from one vertex. It was verified that nearly all the remaining triggers resulted from secondary interactions and photon conversion. The track efficiency computed from missing points on reconstructed tracks was $\sim$ 90% for two-track cases. All events were classified according to their most probable identification. For Λ and K^0 events, this classification could be verified to be more than 95% efficient, as these states were primarily identified by a cut in the distance from the vertex to the interaction point at 50 cm.

The spectrometer acceptance has been computed at the mass peaks by giving a weight to each event according to an assumed isotropic decay spectrum and the probability to capture both decay products. The known branching ratios and decays of secondaries are taken into account. No absolute values of the cross-sections are given yet, but we expect the relative values of the cross-sections for the different states to be correct within a factor of 2.

The $\bar{p}$ data have been taken with 100% field and a SF_6/CO_2 mixture in all Čerenkov counters. The counters Č2 and Č3 were in anticoincidence in the trigger. High-momentum negative particles were selected in the trigger by requiring specific combinations of hodoscope elements to fire. The fraction of tracks reconstructed was 17% of all triggers. The Čerenkov efficiencies and δ-ray contamination were checked in separate runs. The contamination from π^- and K^- in the $\bar{p}$ data shown is less than 1%. Selection of a subclass of events, in which a maximum number of coordinates were required on the tracks, ascertained that the high-momentum low-cross-section part of the $\bar{p}$ spectrum is not populated by wrongly reconstructed lower-momentum tracks. Corrections were made for multiple tracks entering the spectrometer. The absolute value of the $\bar{p}$ cross-sections are estimated to have a systematic error of less than 20%.

The data fill a narrow band in the x p_T plane. The x and p_T dependence has been determined by a fit to a function of the form:

$$A(1-x)^n \exp(-B\, p_T^2) \qquad \text{for } x > 0.6 \ .$$

Factorization between the x and p_T dependence is thus assumed. Data points at fixed p_T are then obtained by extrapolating to p_T = 0.65 GeV/c with the fitted value of B. Below x = 0.6 the Λ data show clear deviations from a simple power law in 1-x. The $\bar{p}$ data have been taken in a limited momentum range, and these are interpolated to p_T = 0.50 GeV/c using a p_T dependence extrapolated from earlier results[2].

4. RESULTS AND DISCUSSION

Mass spectra of the Λ^0, $\bar{\Lambda}^0$ are shown in Fig. 1a, of the $\Lambda^0(1520)$ in Fig. 1b, and of the $\phi(1020)$ in Fig. 1c. The mass resolution determined from Λ and K^0 spectra is 5-10 MeV.

The measured $\bar{\Lambda}^0/\Lambda^0$ ratio is free from most identification and acceptance biases. The result, corrected for background under the peaks, is shown in Fig. 2, along with data from Kichimi et al.[3] and a fit with a function of the form $A(1-x)^n$.

The x-distributions measured for Λ^0, $\Lambda^0(1520)$, and $\phi(1020)$ are shown in Fig. 3.

The invariant cross-section for $\bar{p}$ production is shown in Fig. 4 along with results from other experiments[2,4-6]. A one-power fit in 1-x no longer describes the data for $x > 0.6$. A fit with $A(1-x)^{n_1} + B(1-x)^{n_2}$ with $A = 910 \pm 50$ $\mu b/GeV^2$, $B = 1.5 \pm 0.5$ $\mu b/GeV^2$, $n_1 = 8.9 \pm 0.1$, $n_2 = 2 \pm 0.5$, is shown to describe the data correctly. This situation is similar to the one of the π- and K-meson production data from Singh et al.[7]. The small errors on these data do not permit a description with a one-power fit over a large x-range. Spectator counting rules, however, relate the dynamical mechanism involved in particle production to the global shape of the momentum spectrum of the secondaries; we therefore also fitted all data with a single power.

The powers derived from these fits along with those obtained in an earlier experiment on stable mesons[7] are shown in Table 1[4,8-10]. Some data from lower energy fixed-target experiments have been added for comparison. The right-hand columns show the values of n indicated by spectator counting rules for quark and gluon exchanges as discussed in the companion paper[1]. It is seen that none of the six types of counting rules can account for all types of reactions measured.

The production of ϕ and J/ψ mesons may proceed via quark annihilation. As is shown in Table 1, this reduces the number of spectators to be counted and would account for the smallness of the cross-sections since the process is then OZI-forbidden.

REFERENCES

1. M.M. Block et al., Correlations between high momentum mesons in $p + p \to \pi + \pi + X$ at $\sqrt{s}$ = 63 GeV, Abstract 318 submitted to this conference.
2. M.G. Albrow et al., Phys. Lett. 42B (1972) 279.
3. H. Kichimi et al., KEK preprint 1979.
4. G. Brandenburg et al., Paper on FNAL exp. E118 presented at the Rencontre de Moriond, March 1979.
5. K. Guettler et al., Nucl. Phys. B116 (1976) 77.
6. P. Capiluppi et al., Nucl. Phys. B70 (1974) 1.
7. J. Singh et al., Nucl. Phys. B140 (1978) 189.
8. K.J. Anderson et al., Phys. Rev. Letters 37 (1976) 799.
9. J.G. Branson et al., Phys. Rev. Letters 38 (1977) 1331.
10. R.T. Edwards et al., Phys. Rev. D 18 (1978) 76.

Table 1

Powers n from a fit $A(1-x)^n$ to the data

Particle	n		Counting-rule predictions a)					
			I	II	III	IV	V	VI
Pseudoscalar mesons								
π^+	3.9 ± 0.3							
π^-	4.1 ± 0.4		5	3	3	3	3	1
K^+	3.2 ± 0.3							
K^-	5.8 ± 0.2		9	7	7	5	5	3
Vector mesons								
$\phi(1020)$	2.4 ± 0.9		9	7	7	5	5	3
	4.1 ± 0.4	pBe [8]			OR b)			
J/ψ	2.94 ± 0.32	pBe [8]	3	3	1	3	3	1
	3.44 ± 0.14	pC						
Baryons								
Λ^0	1.5 ± 0.2							
	0.66 ± 0.01	pBe [10]	3	1	0	1	1	0
$\Lambda^0(1520)$	0.8 ± 0.2							
Antibaryons								
$\bar{\Lambda}^0$	10.0 ± 0.8							
	$7.6 \pm 1.7 - 2.4$	pBe [10]	11	9	9	5	5	3
$\bar{p}$	8.3 ± 0.2							
	8.4 ± 0.6	[4]						

a) Counting rule

	Type of quarks counted	Exchange
I	Sea and valence	Gluons
II	"	Sea quarks
III	"	Valence quarks
IV	Valence	Gluons
V	"	Sea quarks
VI	"	Valence quarks

b) Quark annihilation

Figure captions

Fig. 1a : Effective mass spectra of $\pi^- p$ and $\pi^{+-} \bar{p}$ pairs, showing Λ^0 and $\bar{\Lambda}^0$ peaks. The $\bar{p}$ is not uniquely identified.

Fig. 1b : Effective mass spectrum of $K^- p$ pairs, showing a $\Lambda^0(1520)$ peak.

Fig. 1c : Effective mass spectrum of $K^+ K^-$ pairs, showing a $\phi(1020)$ peak.

Fig. 2 : $\bar{\Lambda}^0/\Lambda^0$ particle ratio versus x, derived from the data shown in Fig. 1a.

Fig. 3 : x-distributions of Λ^0, $\bar{\Lambda}^0(1520)$, and $\phi(1020)$ production. The vertical scale is in arbitrary units.

Fig. 4 : x-distribution of $\bar{p}$ production. One- and two-power fits are indicated.

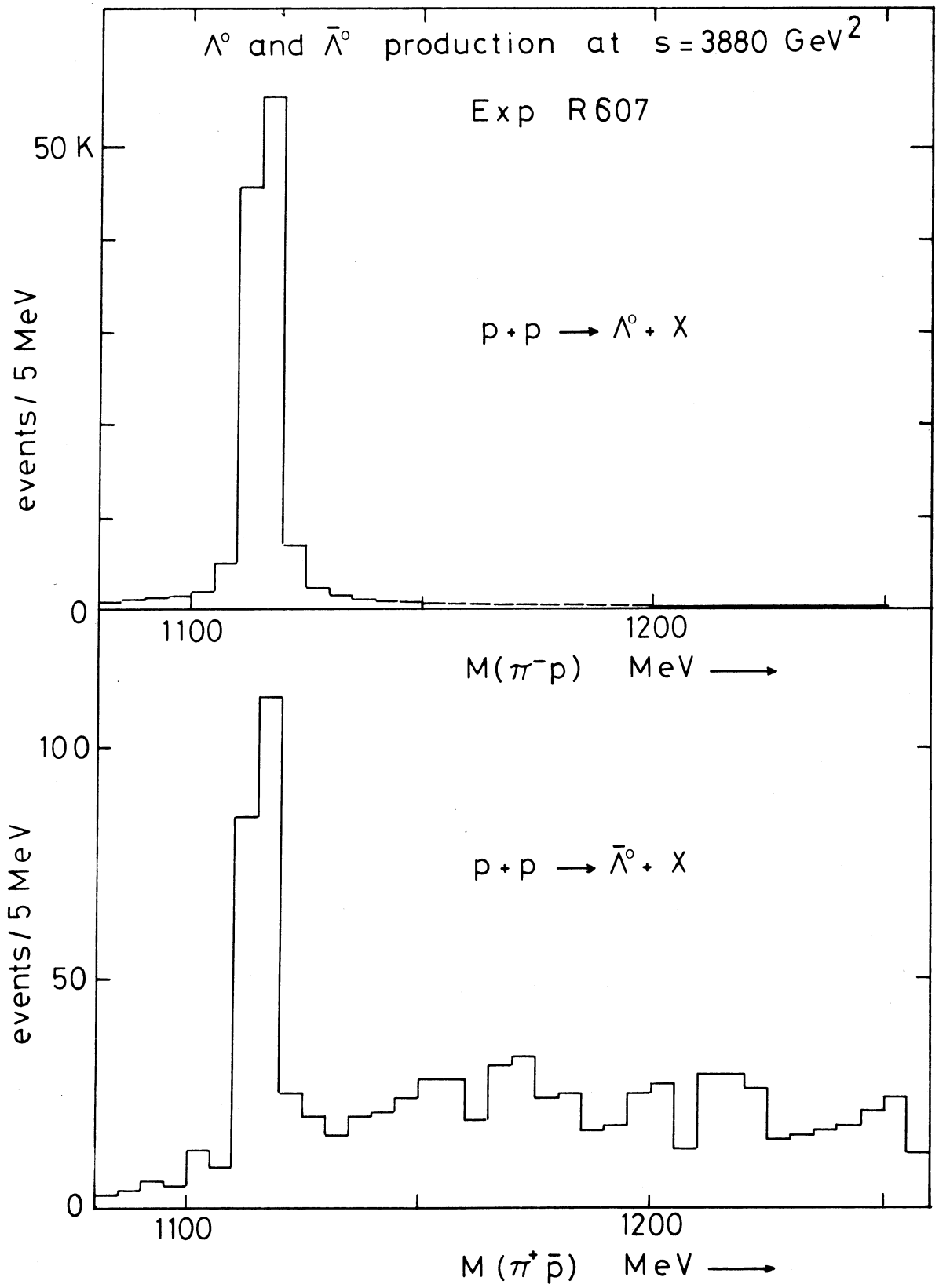
Λ° and Λ̄° production at s = 3880 GeV²
Exp R607
50 K
events / 5 MeV
0
p + p → Λ° + X
1100
1200
M(π⁻p) MeV →
100
50
0
events / 5 MeV
p + p → Λ̄° + X
1100
1200
M (π⁺ p̄) MeV →

Fig. 1a

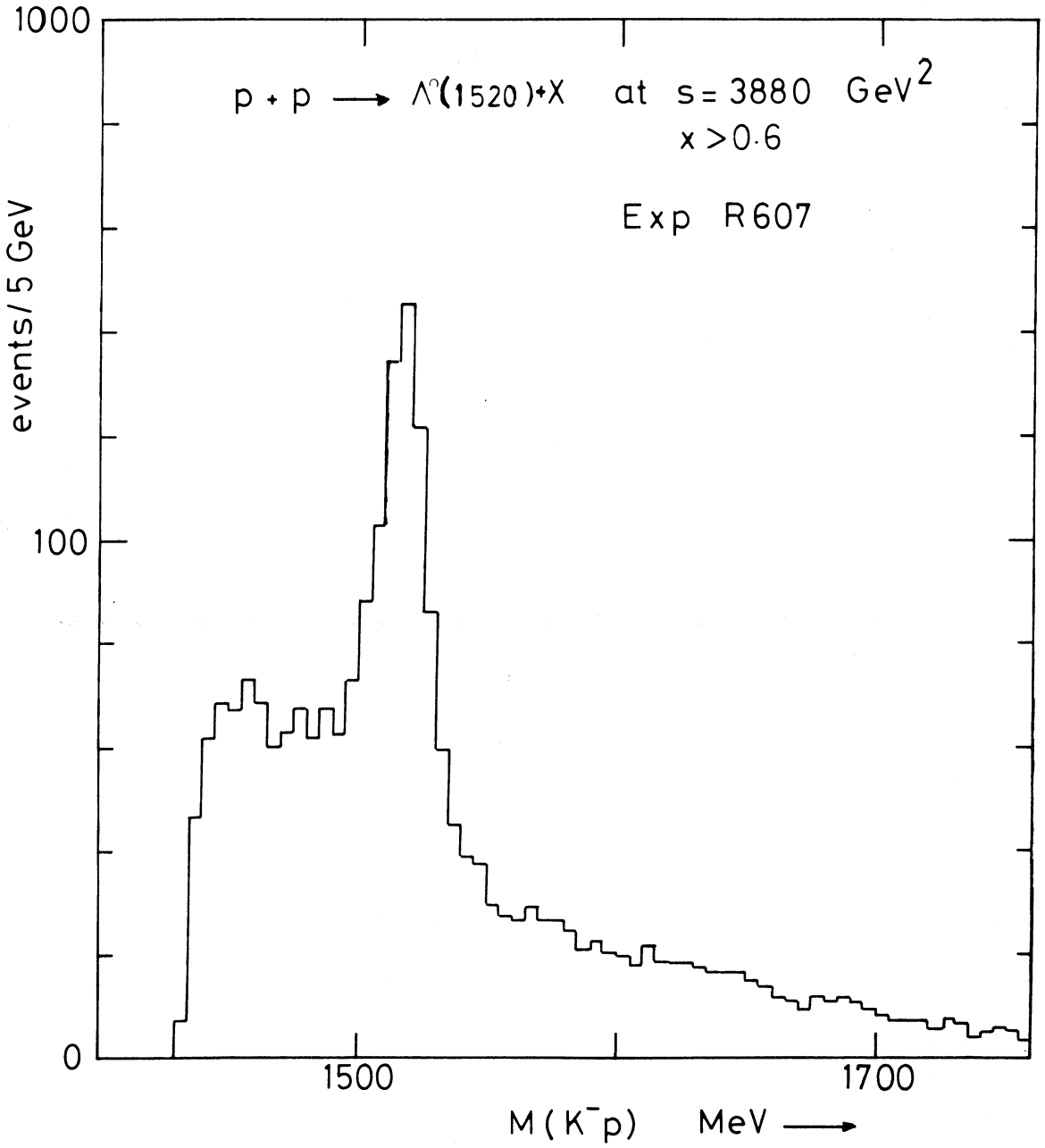
1000
100
0
events/5 GeV
p + p ⟶ Λ°(1520)+X at s = 3880 GeV²
x > 0·6
Exp R607
1500
1700
M(K⁻p) MeV ⟶

Fig. 1b

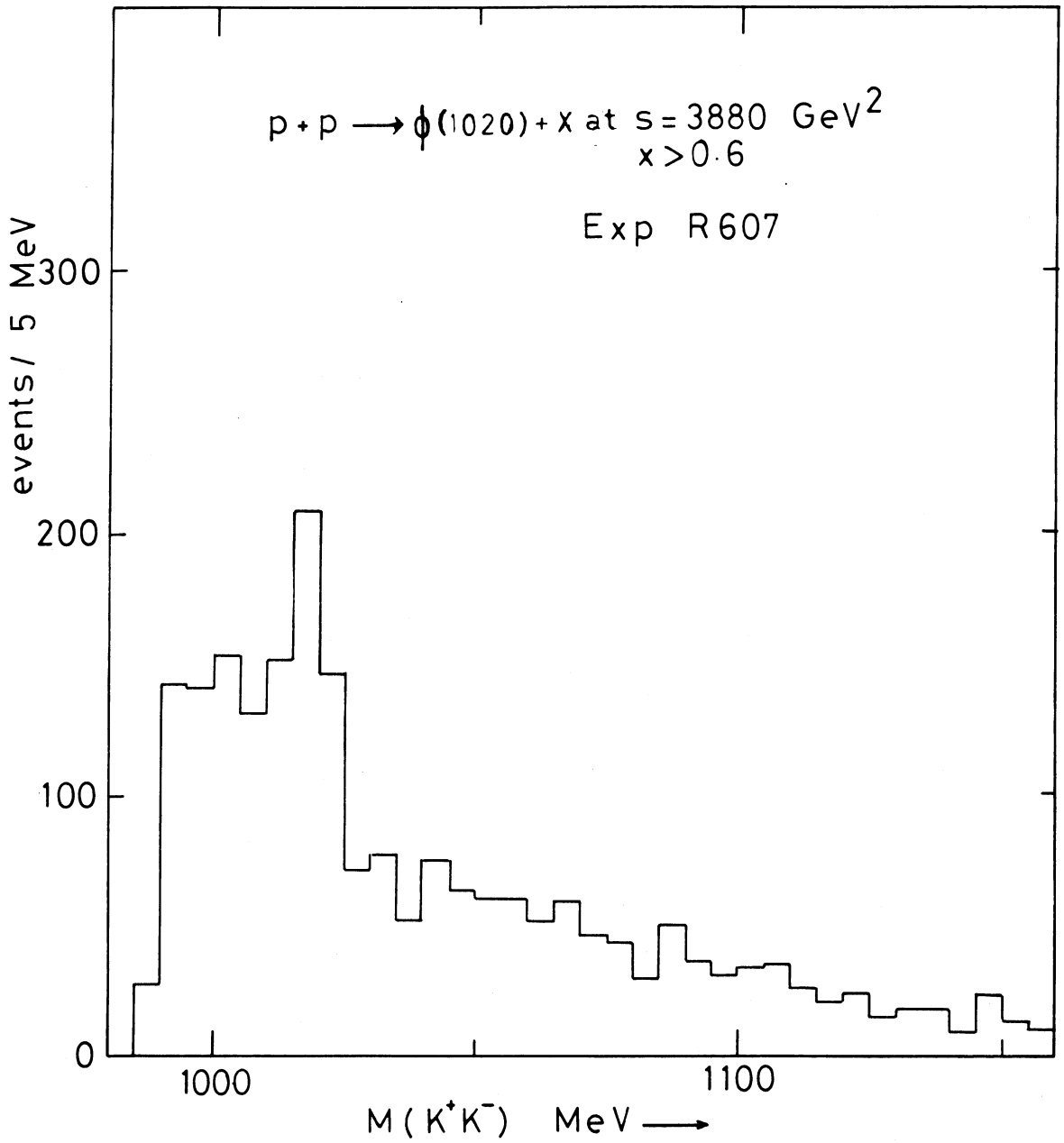
p + p → φ(1020) + X at s = 3880 GeV²
x > 0·6
Exp R607
events / 5 MeV
300
200
100
0
1000
1100
M(K⁺K⁻) MeV →

Fig. 1c

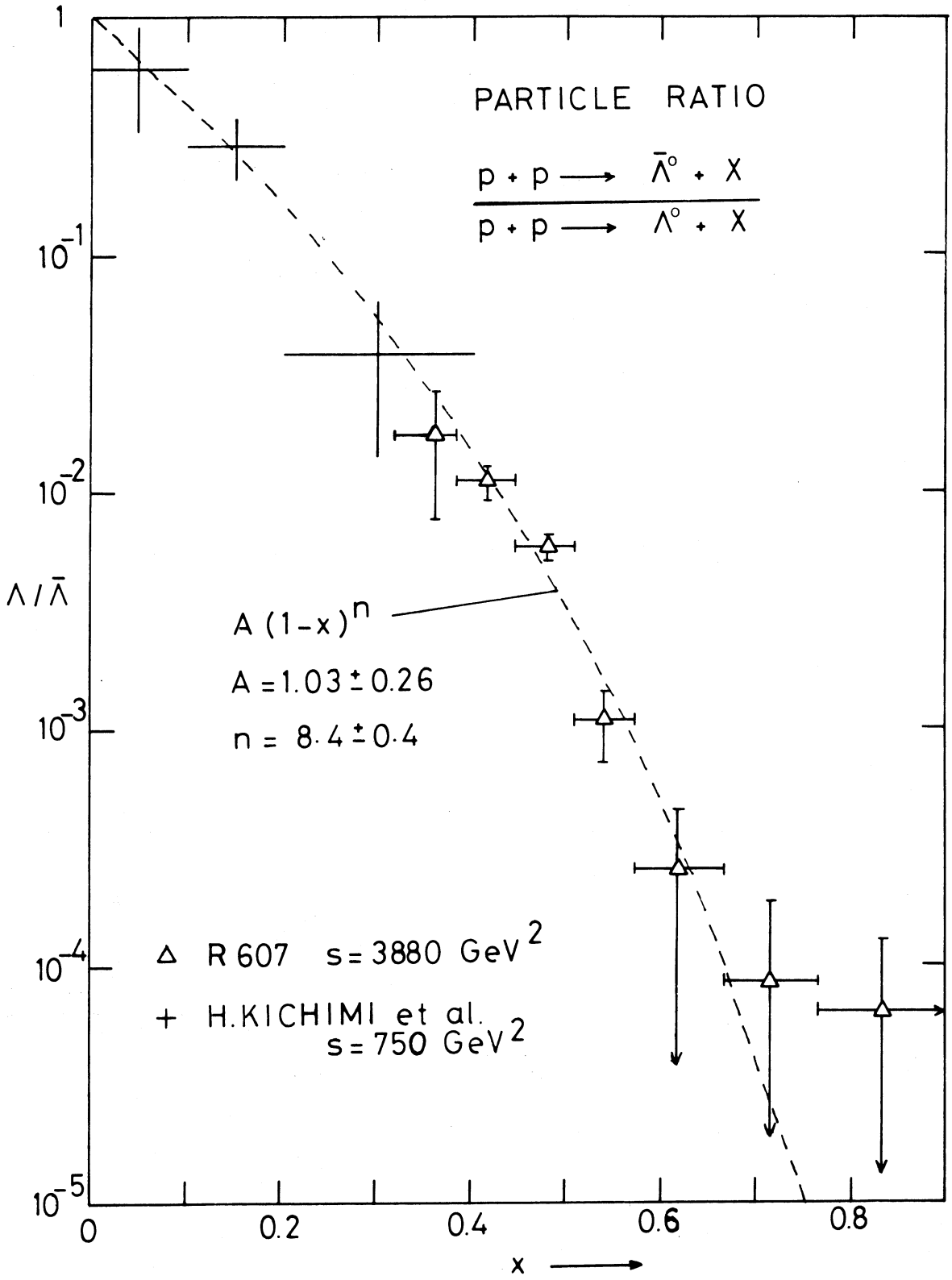
PARTICLE RATIO
p + p → Λ̄° + X
p + p → Λ° + X
A (1-x)^n
A = 1.03 ± 0.26
n = 8.4 ± 0.4
Δ R 607 s = 3880 GeV^2
+ H.KICHIMI et al. s = 750 GeV^2
Λ / Λ̄
x
1
10^-1
10^-2
10^-3
10^-4
10^-5
0
0.2
0.4
0.6
0.8

Fig. 2

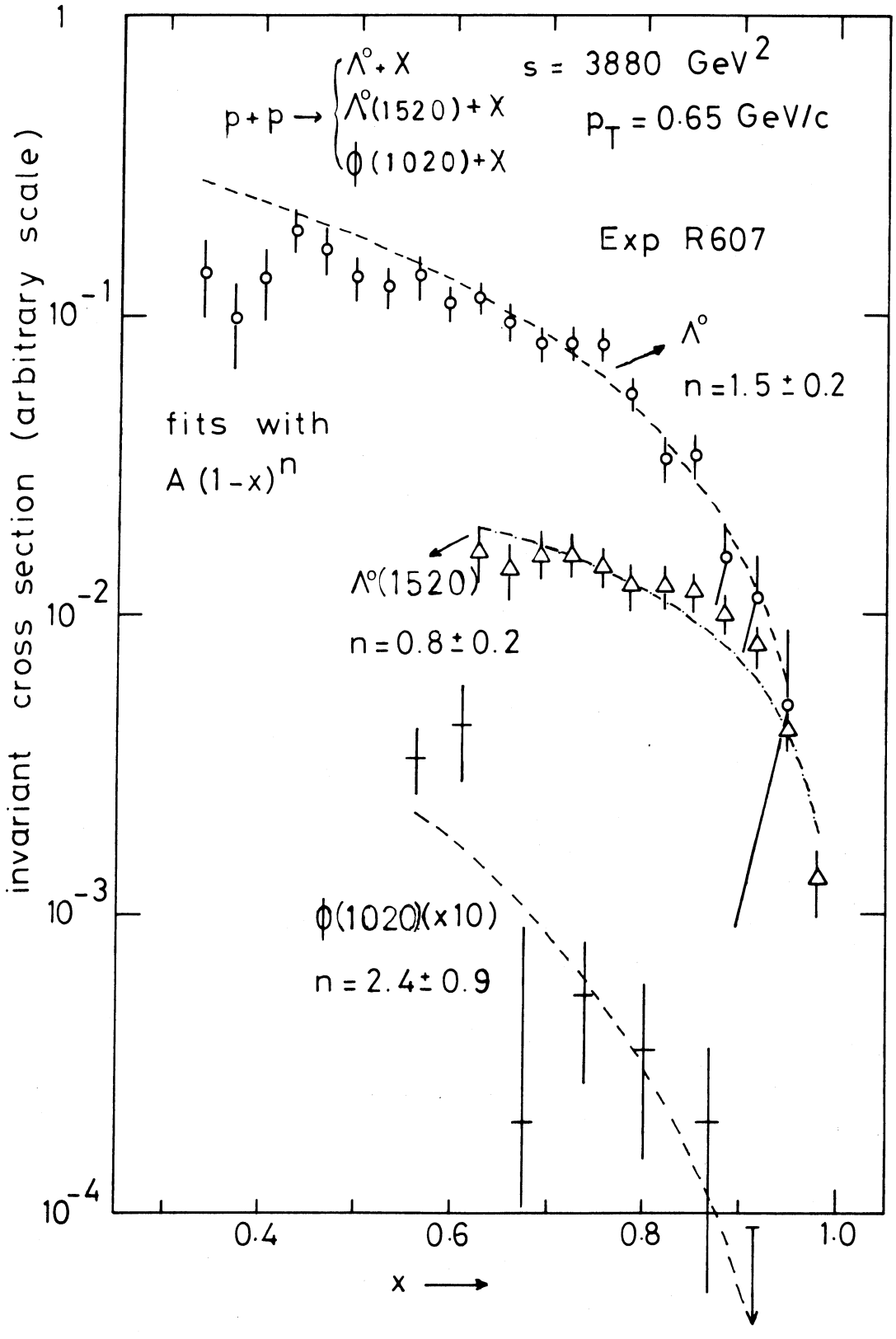
1
10^{-1}
10^{-2}
10^{-3}
10^{-4}
invariant cross section (arbitrary scale)
$p+p \rightarrow \begin{cases} \Lambda^0 + X \\ \Lambda^0(1520) + X \\ \phi(1020) + X \end{cases}$
$s = 3880\ GeV^2$
$p_T = 0.65\ GeV/c$
Exp R607
Λ^0
$n = 1.5 \pm 0.2$
fits with
$A(1-x)^n$
$\Lambda^0(1520)$
$n = 0.8 \pm 0.2$
$\phi(1020)(x10)$
$n = 2.4 \pm 0.9$
0.4
0.6
0.8
1.0
x

Fig. 3

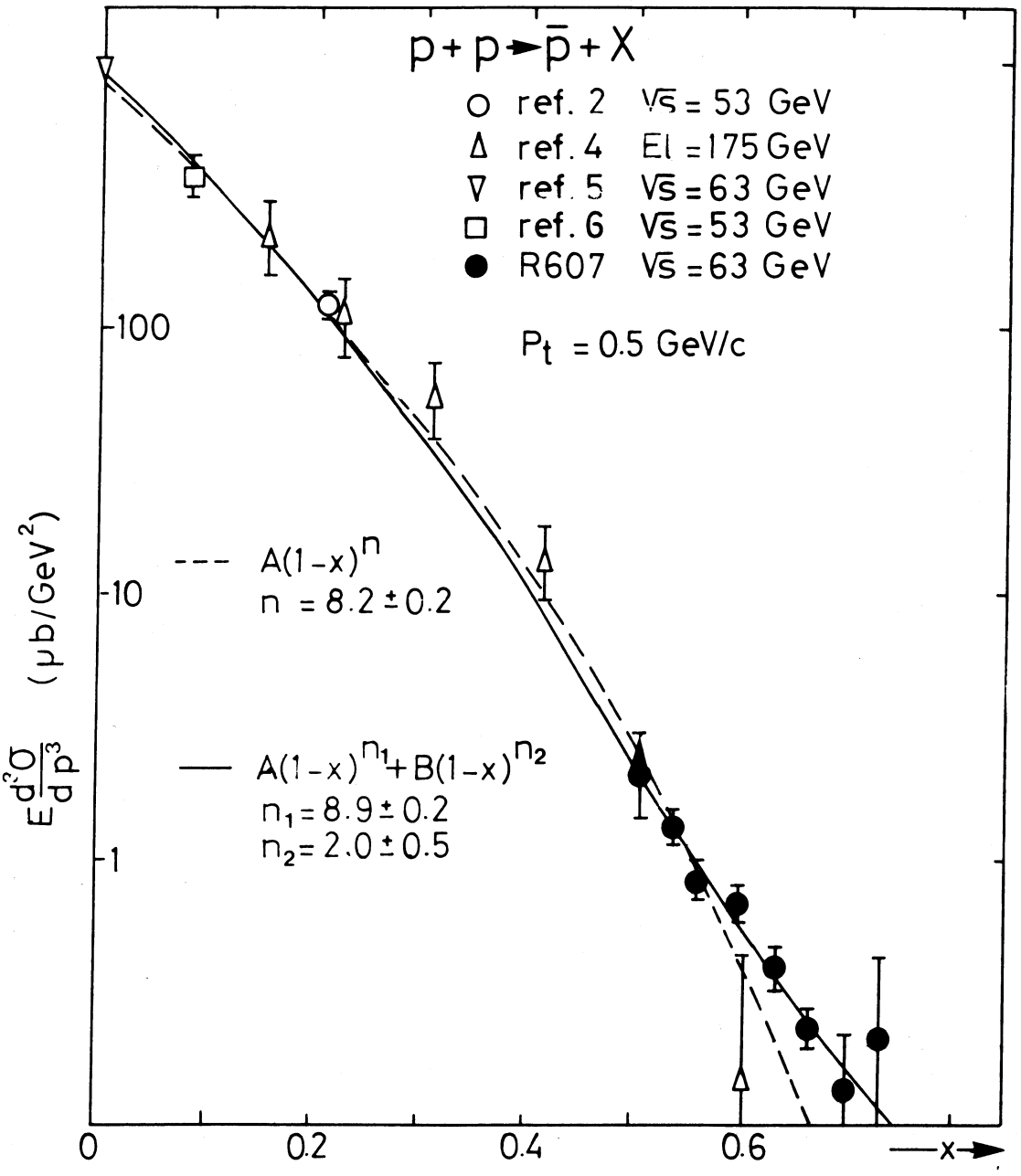
p + p → p̄ + X
ref. 2 √s = 53 GeV
ref. 4 El = 175 GeV
ref. 5 √s = 63 GeV
ref. 6 √s = 53 GeV
R607 √s = 63 GeV
Pt = 0.5 GeV/c
--- A(1-x)^n
n = 8.2 ± 0.2
—— A(1-x)^n1 + B(1-x)^n2
n1 = 8.9 ± 0.2
n2 = 2.0 ± 0.5
E d³σ/dp³ (μb/GeV²)
100
10
1
0
0.2
0.4
0.6
x

Fig. 4